Original Article | Thoracic Imaging

eISSN 2005-8330
https://doi.org/10.3348/kjr.2020.0955
Korean J Radiol 2021;22(5):829-839

Korean Journal of Radiology
KJR

Imaging Assessment of Visceral Pleural Surface Invasion by Lung Cancer: Comparison of CT and Contrast-Enhanced Radial T1-Weighted Gradient Echo 3-Tesla MRI

Yu Zhang[1], Woocheol Kwon[2], Ho Yun Lee[3, 4], Sung Min Ko[1], Sang-Ha Kim[5], Won-Yeon Lee[5], Suk Joong Yong[5], Soon-Hee Jung[6], Chun Sung Byun[7], JunHyeok Lee[8], Honglei Yang[1], Junhee Han[1], Jeanne B. Ackman[9]

Departments of [1]Radiology, [5]Internal Medicine, [6]Pathology, [7]Thoracic and Cardiovascular Surgery, [8]Biostatistics, Yonsei University Wonju College of Medicine, Wonju, Korea; [2]Department of Diagnostic Radiology, College of Medicine, Ewha Womans University, Seoul, Korea; [3]Department of Radiology, Samsung Medical Center, Sungkyunkwan University School of Medicine, Seoul, Korea; [4]Departement of Health Sciences and Technology, Samsung Advanced Institute of Health Sciences and Technology (SAIHST), Sungkyunkwan University, Seoul, Korea; [9]Harvard Medical School, Massachusetts General Hospital, Founders House, Boston, MA, USA

Objective: To compare the diagnostic performance of contrast-enhanced radial T1-weighted gradient-echo 3-tesla (3T) magnetic resonance imaging (MRI) and computed tomography (CT) for the detection of visceral pleural surface invasion (VPSI). Visceral pleural invasion by non-small-cell lung cancer (NSCLC) can be classified into two types: PL1 (without VPSI), invasion of the elastic layer of the visceral pleura without reaching the visceral pleural surface, and PL2 (with VPSI), full invasion of the visceral pleura.

Materials and Methods: Thirty-three patients with pathologically confirmed VPSI by NSCLC were retrospectively reviewed. Multidetector CT and contrast-enhanced 3T MRI with a free-breathing radial three-dimensional fat-suppressed volumetric interpolated breath-hold examination (VIBE) pulse sequence were compared in terms of the length of contact, angle of mass margin, and arch distance-to-maximum tumor diameter ratio. Supplemental evaluation of the tumor-pleura interface (smooth versus irregular) could only be performed with MRI (not discernible on CT).

Results: At the tumor-pleura interface, radial VIBE MRI revealed a smooth margin in 20 of 21 patients without VPSI and an irregular margin in 10 of 12 patients with VPSI, yielding an accuracy, sensitivity, specificity, positive predictive value, negative predictive value, and F-score for VPSI detection of 91%, 83%, 95%, 91%, 91%, and 87%, respectively. The McNemar test and receiver operating characteristics curve analysis revealed no significant differences between the diagnostic accuracies of CT and MRI for evaluating the contact length, angle of mass margin, or arch distance-to-maximum tumor diameter ratio as predictors of VPSI.

Conclusion: The diagnostic performance of contrast-enhanced radial T1-weighted gradient-echo 3T MRI and CT were equal in terms of the contact length, angle of mass margin, and arch distance-to-maximum tumor diameter ratio. The advantage of MRI is its clear depiction of the tumor-pleura interface margin, facilitating VPSI detection.

Keywords: *Magnetic resonance imaging; Lung cancer; Diagnostic imaging*

INTRODUCTION

Visceral pleural invasion (VPI) by non-small-cell lung cancer (NSCLC) can be classified into two types, PL1 and PL2, representing cases without and with visceral pleural surface invasion (VPSI), respectively [1]. The 8th edition

Received: July 27, 2020 **Revised:** November 10, 2020 **Accepted:** November 28, 2020
Corresponding author: Sung Min Ko, MD, PhD, Department of Radiology, Wonju Severance Christian Hospital, Yonsei University Wonju College of Medicine, 20 Ilsan-ro, Wonju 26426, Korea.
• E-mail: ksm9723@yahoo.co.kr

of the TNM classification for lung cancer classifies both invasion of the elastic layer of the visceral pleura without reaching the visceral pleural surface (PL1) and full invasion of the visceral pleura (PL2) as stage T2 [2], suggesting that PL1 and PL2 tumors have similar prognosis and survival [3]. However, a study showed that the 5-year overall survival rate was significantly higher for patients with PL1 tumors (61.9%) than for those with PL2 tumors (39.2%) [4]. The 5-year survival rates of patients with and without VPSI were 57.9% and 83.0%, respectively, for N0–N2 disease and 74.3% and 88.5%, respectively, for N0 disease [1]. VPSI might therefore be considered an independent risk factor for poor prognosis, and its presence might be a potential indication for adjuvant chemotherapy [1].

Computed tomography (CT) is a noninvasive imaging modality for preoperative staging of lung cancers. However, it has limitations in the detection of more subtle cases of pleural invasion, as contiguity of the tumor with the pleural surface is not necessarily equivalent to its invasion [5]. A skirt-like 3-dimensional (3D) CT pattern of pleural morphology adjacent to the tumor [6], pleural tag with a soft tissue component [7], and type-5 border (convex border with a perpendicular or blunt angle) [8] have been shown to have predictive value for pleural invasion; however, these methods cannot be used to differentiate PL1 from PL2.

Magnetic resonance imaging (MRI) is potentially advantageous for VPSI detection because of its superior soft tissue contrast and tissue characterization properties, without ionizing radiation exposure. Conventional MRI can yield high-quality images of the thorax, particularly with breath-hold techniques; however, breath-holding can be challenging for some patients. Free-breathing, intravenous contrast-enhanced, radial, 3D ultrafast gradient-echo (volumetric interpolated breath-hold examination [VIBE]) T1-weighted imaging, hereinafter referred to as "radial VIBE," has been proposed as an alternative to breath-hold post-contrast imaging. It enables patients to breathe freely during scanning, yielding excellent image quality and diagnostic performance owing to the enhanced lesion conspicuity, clarity of the tumor interface, and reduced respiratory motion artifacts compared to other free-breathing techniques [9,10].

Moreover, this sequence has been proven to be useful for evaluating the morphological features of lung cancer and for readily demonstrating the tumor-pleura interface [11]. Therefore, this study aimed to compare the diagnostic performance of contrast-enhanced, radial VIBE 3-tesla (3T) MRI, and CT for VPSI detection.

MATERIALS AND METHODS

This retrospective, bi-institutional study was conducted at Wonju Severance Christian Hospital and Samsung Medical Center. The study was approved by the Institutional Review Boards of both institutions and the local ethics committee (IRB No. CR319094). The requirement for written informed consent was waived.

Patients

Initially, 191 consecutive lung cancer patients who underwent both CT and 3T MRI between January 2016 and May 2019 were enrolled. Patients with poor quality CT or MRI scans were excluded (Fig. 1). Finally, a total of 33 patients met the following inclusion criteria: 1) nonmetastatic, primary NSCLC treated with surgical resection; 2) available pathology reports describing the extent of pleural invasion; 3) preoperative CT and 3T MRI scans with the same scan parameters available on a picture archiving and communication system (PACS); 4) available

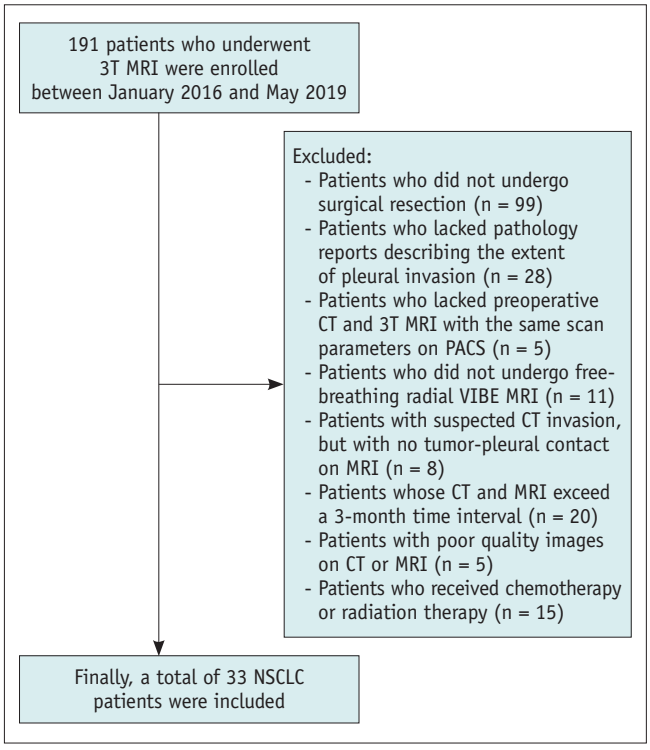

Fig. 1. Flowchart illustrating patient selection. CT = computed tomography, MRI = magnetic resonance imaging, NSCLC = non-small-cell lung cancer, PACS = picture archiving and communication system, VIBE = volumetric interpolated breath-hold examination, 3T = 3-tesla

https://doi.org/10.3348/kjr.2020.0955

Korean Journal of Radiology
KJR

free-breathing fat-saturated radial VIBE sequence on MRI; 5) suspected pleural invasion on CT; 6) CT and MRI performed within 3 months; and 7) no prior or current chemotherapy or radiation therapy. The sample including 23 patients from the Blinded Hospital and 10 from the Blinded Medical Center was comprised of 28 male and five female, aged 46–88 years (mean age, 68 ± 10 years). This study analyzed 17 adenocarcinomas, 13 squamous cell carcinomas, and three large cell carcinomas (Table 1).

CT Scanning

A 64-channel multidetector CT scanner (Brilliance 64, Philips Medical System) was used at both institutions for breath-hold imaging in the supine position, with a 7–8 second breath-hold. The technical parameters of the CT scans were as follows: 0.625-mm detector collimation, 512 x 512 matrix, 340-mm field-of-view, 80–120-mAs tube current, 120-kV tube voltage, 2.5-mm slice thickness, and 0.5-seconds rotation time. For each patient, 350 mg/mL iohexol contrast material was administered intravenously at a rate of 2.5 cc/s [11].

Table 1. Clinicopathologic Features of Non-Small-Cell Lung Cancer Patients in This Study

Clinicopathologic Features	Data
No. of patients	33
Age, years, mean ± SD (46–88)	68.33 ± 9.96
Sex, n (%)	
Male	28 (84.8)
Female	5 (15.2)
Tumor size, mm, mean ± SD	53.4 ± 26.2
Tumor pathology, n (%)	
Adenocarcinoma	17 (51.5)
Squamous cell carcinoma	13 (39.4)
Large cell carcinoma	3 (9.1)
Tumor location, n (%)	
RUL	11 (33.3)
RML	1 (3.0)
RLL	12 (36.4)
LUL	3 (9.1)
LLL	6 (18.2)
T stage, n (%)	
T1	1 (3.0)
T2	14 (42.4)
T3	12 (36.4)
T4	6 (18.2)
Pleural invasion grade, n (%)	
PL0	11 (33.3)
PL1	10 (30.3)
PL2	3 (9.1)
PL3	9 (27.3)

LLL = left lower lobe, LUL = left upper lobe, RLL = right lower lobe, RML = right middle lobe, RUL = right upper lobe

MRI Scanning

All MRI examinations were performed using a 3T system (MAGNETOM Skyra) with a 60-channel body coil. Patients were imaged in the supine position with their arms overhead to eliminate potential artifacts from the arms positioned on each side. The following pulse sequences were used in 23 patients: axial breath-hold T1- and T2-weighted turbo spin echo, axial T2-weighted half-Fourier acquisition single-shot turbo spin echo, contrast-enhanced fat-saturated T1-weighted, and contrast-enhanced free-breathing, fat-saturated radial VIBE. The pulse sequences common to all included patients were breath-hold T1-weighted and contrast-enhanced free-breathing fat-suppressed radial VIBE. Gadoteridol (0.1 mmoL/kg; Pro-Hance; Bracco Imaging) was injected at a rate of 1.5 cc/s. The radial VIBE imaging parameters with an isotropic resolution of 0.9 mm were as follows: repetition time, 3.36 ms; echo time, 1.66 ms; flip angle, 5°; field of view, 260 mm x 260 mm; and matrix size, 288 x 288 mm.

Imaging Analysis

Two chest radiologists (readers 1 and 2, with 23 and 3 years of clinical experience, respectively), who were blinded to the patients' clinical information and pathological results, evaluated the CT and MRI scans by consensus. To make the final decision, the radiologists were allowed to refer to the images several times and adjust the window and level settings if necessary. The observers were instructed to read all CT scans first, followed by MRI scans after 1 month to avoid interference bias between CT and MRI results in interpretation.

Tumor size (maximum dimension in any of the three planes [axial, sagittal, and coronal]) on CT and MRI scans, and tumor location were recorded. The angle of the mass margin was formed from the center of the tumor toward both ends of the pleural contact. The length of pleural contact was the length of the interface between the primary tumor and the pleura. It was drawn freehand and measured in the same image (Fig. 2B) [12,13]. The arch distance to maximum tumor diameter ratio was the length of the interface between the primary tumor and the neighboring structure (in this case, the pleura) (Fig. 2B) [14]. The imaging criteria utilized to determine the degree of

https://doi.org/10.3348/kjr.2020.0955

suspicion for VPI were as follows (Fig. 2A): a high suspicion for VPI required a length of pleural contact > 5 cm or a > 180° angle between the margin of the mass and the pleural surface; moderate suspicion of VPI required a 3–5 cm contact length or a 90°–180° angle between the mass and the pleural surface; and mild suspicion of pleural invasion required a length of pleural contact < 3 cm or angle of mass margin < 90°.

Based on the smoothness or irregularity of the high signal intensity band interface between the tumor and the pleura, MRI scans were classified into two groups (Fig. 3): without VPSI, with smooth and clear margins, well-defined curvilinear pleural enhancement, and absence of protrusion of the interface between the tumor and the pleura (Fig. 3A); and with VPSI, with an irregular, undulating, or coarse margin or protrusion of the interface between the primary tumor and the pleura (Fig. 3B). The two groups were assessed in the axial, sagittal, and coronal planes. VPSI was determined if an irregular interface was observed in any plane. The lung cancer was deemed to be without VPSI only when there was a smooth tumor-pleura interface in all three planes.

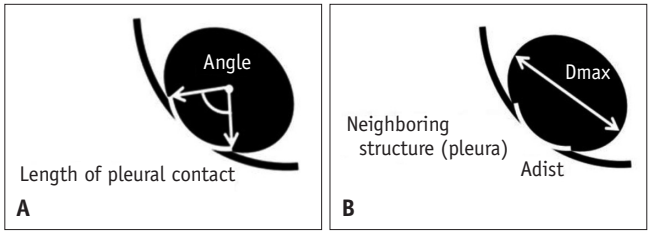

Fig. 2. Measurement of the angle between the margin of the mass and the pleural surface and arch distance-to-maximum tumor diameter ratio on the CT images.
A. Measurement of the angle between the margin of the mass and the pleural surface on CT. The length of pleural contact was drawn freehand. The angle formed by the center of the mass and the two ends of the length of pleural contact is the "angle of mass margin." **B.** Measurement of the arch distance-to-maximum tumor diameter ratio on the CT image of a pathologically determined PL2. Arch distance is defined as the length of the interface between the primary tumor and a neighboring structure, which, in this case, is the pleura [14]. The arch distance was drawn freehand and measured in the same image. Subsequently, the arch distance-to-maximum tumor diameter ratio was calculated. CT = computed tomography

Pathological Analysis

Pathological specimens were stained with the Verhoeff-Van Gieson stain to investigate the presence and extent of pleural invasion. A pathologist with 33 years of experience in analyses of lung specimens performed the analysis and staged the pleural invasion in each patient as follows: PL0, no pleural invasion; PL1, tumor invasion beyond the elastic layer of the visceral pleura but not the surface of the visceral pleura; PL2, tumor invasion of the surface of the visceral pleura; and PL3, tumor invasion of the parietal pleura or chest wall [15].

Statistical Analysis

Patient age and tumor size were assessed using the Wilcoxon rank-sum test. Sex, tumor pathology, and tumor location were assessed using Fisher's exact test between the two groups. Kappa statistics for categorical data were used to determine interobserver agreement. The Kappa result was interpreted as follows: < 0.20, slight; 0.21–0.40, fair; 0.41–0.60, moderate; 0.61–0.80, substantial; and

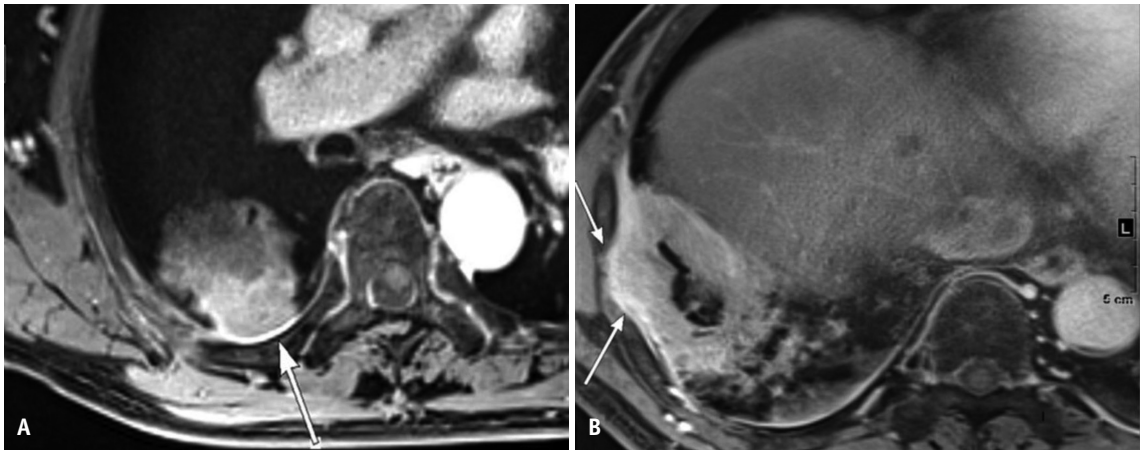

Fig. 3. Lung cancer without and with VPSI.
A. Right lower lobe lung adenocarcinoma without VPSI in a 69-year-old female shows a smooth and clear margin, with well-defined curvilinear pleural enhancement (arrow) and absence of protrusion of the tumor into the pleura. **B.** Right lower lobe squamous cell carcinoma with VPSI in a 76-year-old male shows an irregular, undulating, or coarse margin or protrusion of the tumor (arrows) at the interface between tumor and pleura. VPSI = visceral pleural surface invasion

https://doi.org/10.3348/kjr.2020.0955

Korean Journal of Radiology
KJR

> 0.81, excellent [16]. The chi-square or Fisher's exact test for categorical data and Wilcoxon rank-sum test for continuous data were used to examine the significant differences between patients with and without VPSI. A p value < 0.05 was considered statistically significant. The diagnostic accuracy, sensitivity, specificity, positive predictive value (PPV), negative predictive value (NPV), and F-score were calculated separately. The accuracies of MRI and CT for evaluating the length of contact and arch distance to maximum tumor diameter ratio were compared using the McNemar test. The receiver operating characteristic (ROC) curve analysis was used to assess the diagnostic values of CT and MRI for VPSI detection, and the area under the curve was calculated. All data analyses were performed using the SAS version 9.4 (SAS Institute Inc.).

RESULTS

The histopathological diagnoses of NSCLCs were as follows: 17 adenocarcinomas, 13 squamous cell carcinomas, and three large cell carcinomas. There were 11 tumors in the right upper lobe, one in the right middle lobe, 12 in the right lower lobe, three in the left upper lobe, and six in the left lower lobe (Table 1).

There were 21 patients without VPSI and 12 patients with VPSI, as determined pathologically. The mean and median tumor size of lung cancer were 49.7 ± 17.9 mm and 44 (33–55) mm, respectively, in the group without VPSI and 61.6 ± 24.2 mm and 55 (38.5–85) mm, respectively, in the group with VPSI. Although a larger tumor diameter was observed in patients with VPSI than in those without, tumor size was not significantly different between the two groups (p = 0.170). There was no significant difference between the two groups in patient age, sex, tumor pathology, or tumor location (Table 2). Tables 3 and 4 show the p value, accuracy, sensitivity, specificity, PPV, NPV, and F-score for the length of contact, angle of mass margin, and arch distance-to-maximum on CT and MRI. The McNemar test showed no significant difference (p > 0.05) in the accuracy of the contact length (MRI, 67%; CT, 61%), angle of mass margin > 90° (both MRI and CT, 61%), or arch distance to maximum tumor diameter ratio > 0.9 (CT, 67%; MRI, 61%) between CT and MRI (Table 5). Moreover, there was no significant difference in the area under the ROC curve for VPSI detection between CT and MRI, suggesting that the diagnostic performances of CT and MRI were similar (Fig. 4) regarding these characteristics.

Examination of the high-signal-intensity band interface between the tumor and the pleura on MRI revealed a smooth margin in 20 of 21 (95.2%) patients without VPSI and an irregular or coarse margin in 10 of 12 (83.3%) patients with VPSI. Similar signs in patients with and without VPSI were not appreciable on CT (Figs. 3, 5). The interface on MRI with the radial VIBE sequence significantly differed between patients with and without VPSI (p < 0.001) (Table 3), and sensitivity, specificity, accuracy, PPV, NPV, and F-score were 83%, 95%, 91%, 91%, 91%, and 87%, respectively. The Kappa value of the comparison between

Table 2. Comparison of Clinicopathologic Features of Non-Small-Cell Lung Cancer Patients without and with VPSI

Variables	Without VPSI† (n = 21)	With VPSI‡ (n = 12)	*P*
Age, years, median (Q1–Q3)	72 (64–77)	65 (54–73)	0.060
Sex, n (%)			0.133*
Male	16 (76.2)	12 (100.0)	
Female	5 (23.8)	0 (0.0)	
Tumor size (mm), median (Q1–Q3)	44 (33–55)	55 (38.5–85)	0.170
Tumor pathology, n (%)			0.215*
Adenocarcinoma	12 (57.1)	5 (41.6)	
Squamous cell carcinoma	8 (38.1)	5 (41.7)	
Large cell carcinoma	1 (4.8)	2 (16.7)	
Location, n (%)			0.106*
RUL	6 (28.6)	5 (41.7)	
RML	1 (4.8)	0 (0.0)	
RLL	9 (42.9)	3 (25.0)	
LUL	0 (0.0)	3 (25.0)	
LLL	5 (23.8)	1 (8.3)	

*Fisher's exact test, †Includes PL0 and PL1, ‡Includes PL2 and PL3. LLL = left lower lobe, LUL = left upper lobe, RLL = right lower lobe, RML = right middle lobe, RUL = right upper lobe, VPSI = visceral pleural surface invasion

https://doi.org/10.3348/kjr.2020.0955

Table 3. CT and MRI Findings in Non-Small-Cell Lung Cancer Patients Without and with VPSI

Variables	Pathology		
	Without VPSI* (n = 21)	With VPSI† (n = 12)	*P*
Tumor size, mm, median (Q1–Q3)			
CT	44 (32.1–54.9)	51 (41.7–82.7)	0.159
MRI	45 (34.6–60.3)	54 (44.2–77.9)	0.165
Length of contact, n (%)			
CT (cm) ≤ 3 vs. > 3			0.133*
≤ 3	10 (47.6)	2 (16.7)	
> 3	11 (52.4)	10 (83.3)	
CT (cm) ≤ 5 vs. > 5			0.149*
≤ 5	16 (76.2)	6 (50.0)	
> 5	5 (23.8)	6 (50.0)	
MRI (cm) ≤ 3 vs. > 3			0.005*
≤ 3	10 (47.62)	0 (0.0)	
> 3	11 (52.38)	12 (100.0)	
MRI (cm) ≤ 5 vs. > 5			0.274
≤ 5	15 (71.4)	6 (50.0)	
> 5	6 (28.6)	6 (50.0)	
Angle of mass margin, n (%)			
CT (°) ≤ 90 vs. > 90			0.030*
≤ 90	8 (38.1)	0 (0.0)	
> 90	13 (61.9)	12 (100.0)	
CT (°) ≤ 180 vs. > 180			0.538*
≤ 180	20 (95.2)	10 (83.3)	
> 180	1 (4.8)	2 (16.7)	
MRI (°) ≤ 90 vs. > 90			0.030*
≤ 90	8 (38.1)	0 (0.0)	
> 90	13 (61.9)	12 (100.0)	
MRI (°) ≤ 180 vs. > 180			0.538*
≤ 180	20 (95.2)	10 (83.3)	
> 180	1 (4.8)	2 (16.7)	
Arch distance-to-maximum tumor diameter ratio, n (%)			
CT			0.041
≤ 0.9	13 (61.9)	3 (25)	
> 0.9	8 (38.1)	9 (75)	
MRI			0.188
≤ 0.9	12 (57.1)	4 (33.3)	
> 0.9	9 (42.9)	8 (66.7)	
Interface between the primary tumor and the pleura, n (%)			< 0.001*
Smooth and clear margin	20 (95.2)	2 (16.7)	
Irregular or coarse margin	1 (4.8)	10 (83.3)	

*Includes PL0 and PL1, †Includes PL2 and PL3. CT = computed tomography, MRI = magnetic resonance imaging, VPSI = visceral pleural surface invasion

the pathology and MRI was substantial at 0.800 for the radial VIBE sequence (Table 4).

DISCUSSION

This study showed that contrast-enhanced 3T MRI with the free-breathing fat-saturated radial VIBE sequence was superior to CT in depicting and distinguishing NSCLCs without VPSI from those with VPSI. VPSI is an independent factor for the poor prognosis of patients with NSCLCs and can influence the T stage, treatment, and prognosis [3]. Therefore, determining VPSI and the depth of pleural

https://doi.org/10.3348/kjr.2020.0955

Korean Journal of Radiology
KJR

Table 4. Comparison of CT and MRI Findings for Prediction of Visceral Pleural Surface Invasion, with Pathology as the Reference Standard

Variables	Accuracy (%)	Sensitivity (%)	Specificity (%)	PPV (%)	NPV (%)	F-Score	Kappa
Length of contact							
CT (cm)							
> 3	61	83	48	48	83	61	0.2667
> 5	67	50	76	55	73	52	0.2667
MRI (cm)							
> 3	67	100	48	52	100	69	0.3980
> 5	64	50	71	50	71	50	0.2143
Angle of mass margin							
CT (°)							
> 90	61	100	38	48	100	65	0.3092
> 180	67	17	95	67	67	27	0.1418
MRI (°)							
> 90	61	100	38	48	100	65	0.3092
> 180	67	17	95	67	67	27	0.1418
Arch distance-to-maximum tumor diameter ratio							
CT (> 0.9)	67	75	62	53	81	62	0.3388
MRI (> 0.9)	61	67	57	47	75	55	0.2186
Interface							
MRI	91	83	95	91	91	87	0.8000

CT = computed tomography, MRI = magnetic resonance imaging, NPV = negative predictive value, PPV = positive predictive value

Table 5. Agreement Between Radial Volumetric Interpolated Breath-Hold Examination Magnetic Resonance Imaging and Computed Tomography When the Same Methods Were Employed

Variables	Kappa Coefficient	McNemar Test (*P*)
Length of contact (> 3 cm)	0.7284	0.317
Length of contact (> 5 cm)	0.9333	0.317
Angle of mass margin (> 90°)	1.0000	-
Angle of mass margin (> 180°)	1.0000	-
Arch distance-to-maximum tumor diameter ratio (> 0.9)	0.8787	> 0.999

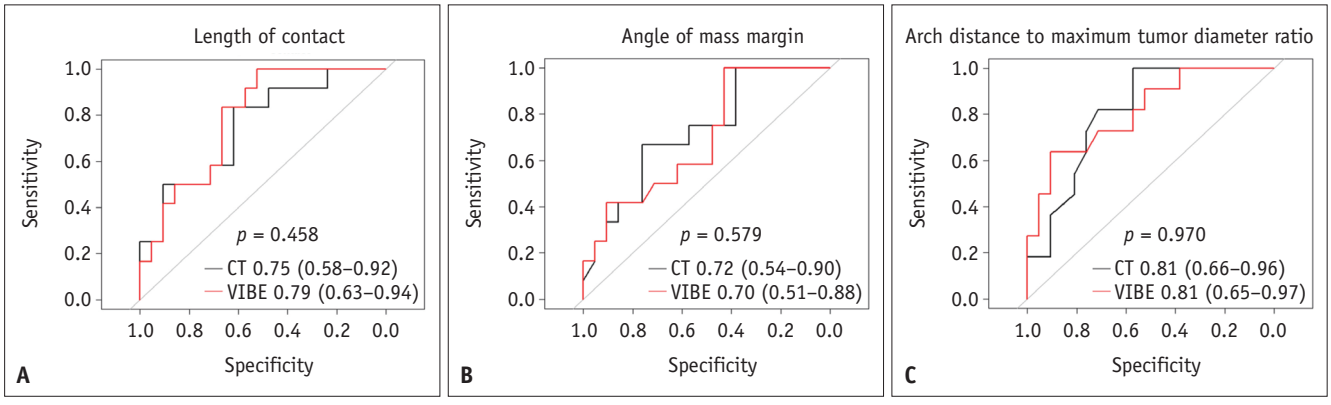

Fig. 4. Summarized receiver operating characteristic curves demonstrating the area under the curve of 75% (95% CI: 58–92%), 72% (95% CI: 54–90%), 81% (95% CI: 66–96%) for CT and 79% (95% CI: 63–94%), 70% (95% CI: 51–88%), 81% (95% CI: 65–97%) for magnetic resonance imaging in the diagnosis of visceral pleural surface invasion on length of contact (A), angle of mass margin (B) and arch distance to maximum tumor diameter ratio (C), respectively. CI = confidence interval, CT = computed tomography, VIBE = volumetric interpolated breath-hold examination

https://doi.org/10.3348/kjr.2020.0955

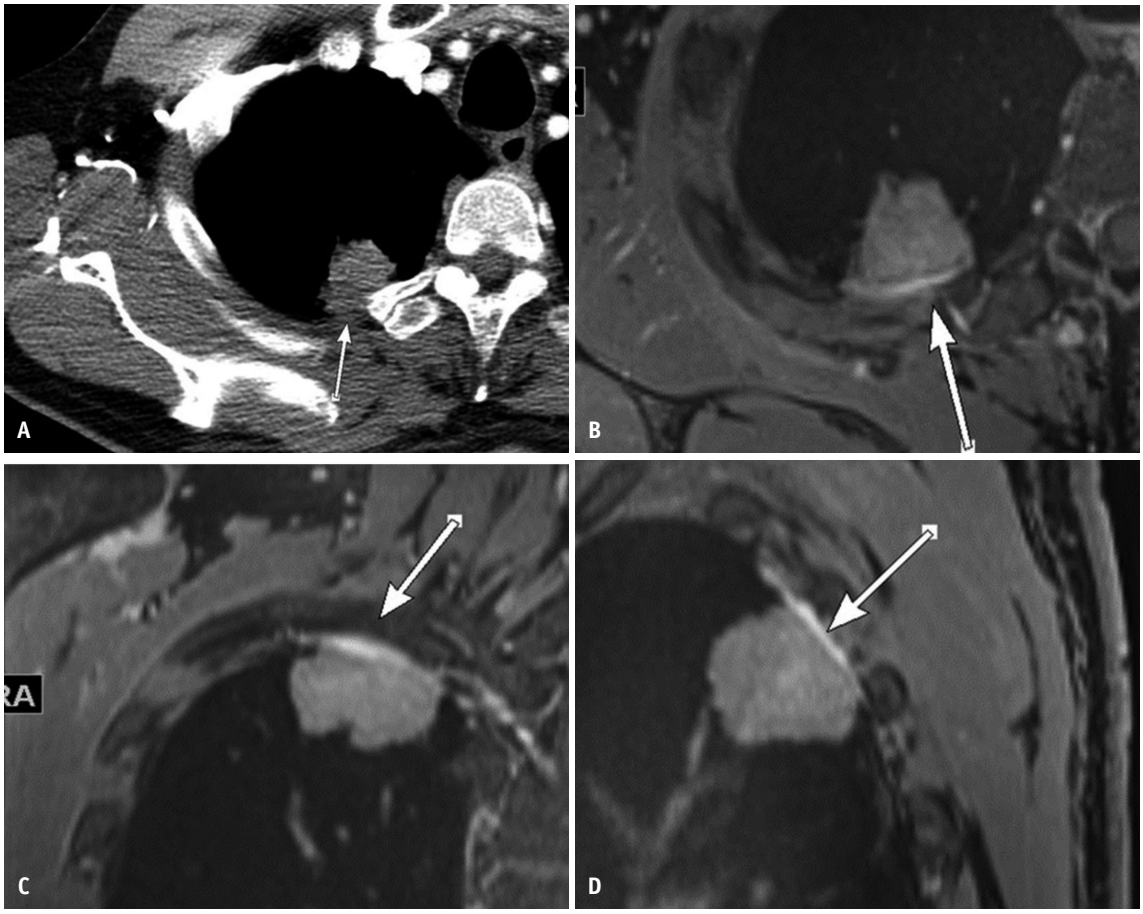

Fig. 5. A 61-year-old male with right lower lobe lung adenocarcinoma and no visceral pleural surface invasion (PL0, as determined pathologically).
A. Contrast-enhanced axial CT shows an ambiguous, blurred interface between the tumor and the pleura (arrow) highlighting the difficulty of evaluation of pleural invasion by CT. **B-D. (B)** Post-contrast free-breathing radial volumetric interpolated fat-saturated image shows a smooth and clear margin, with well-defined curvilinear pleural enhancement (arrows), and absence of protrusion at the interface between the tumor and the pleura in the axial, **(C)** coronal, and **(D)** sagittal planes. CT = computed tomography

invasion is important [6]. To predict pleural invasion, several radiological tools have been used in recent years. Chest radiography, which is the most common modality for the initial investigation of lung disease, is unsuitable for the assessment of pleural invasion [17]. Although CT is widely used for staging lung cancers, its ability to predict pleural invasion is limited [2]. Dynamic free-breathing steady-state free precession MRI has been used to assess the movement of a tumor abutting the chest wall during breathing with 88.5% accuracy [18]. The whole-lesion histogram analysis of the apparent diffusion coefficient could assist in the assessment of pleural invasion [19]. However, to the best of our knowledge, no previous studies have distinguished PL1 from PL2 pleural invasion. Our results showed that the interface between the tumor and the pleura is a useful MRI marker for the determination of VPSI with 91% accuracy. CT and MRI were equivalent in terms of the other parameters examined. There were no significant differences in the areas under the ROC curve between CT and MRI for the contact length, angle of mass margin, or arch distance-to-maximum tumor diameter ratio.

Elastic fiber staining is an important and widely accepted pathological technique for the detection and assessment of pleural invasion by lung cancer [15]. However, a previous study has highlighted the difficulties and even the impracticality of clearly classifying the depth of tumor invasion on histological slices when relying on identification of small and sometimes barely visible structures, such as the lamina elastica interna [20]. Elastic stains may be helpful for identifying the visceral pleural surface in cases of adhered visceral and parietal pleurae [16]. Although the application of elastic stains is simple and inexpensive, interpretation of the histologic results can be challenging [21]. This study showed MRI to be a potential

https://doi.org/10.3348/kjr.2020.0955

Korean Journal of Radiology
KJR

non-invasive, non-radiative adjunct for this assessment.

In this study, the free-breathing radial VIBE sequence depicted a high-signal-intensity band at the interface between the tumor and the pleura. The smoothness or irregularity of this interface distinguished tumors without and with VPSI with substantial accuracy (Figs. 3, 5, 6). This high-signal-intensity band has been shown to correspond pathologically to edematous, thickened, adhered pleura,

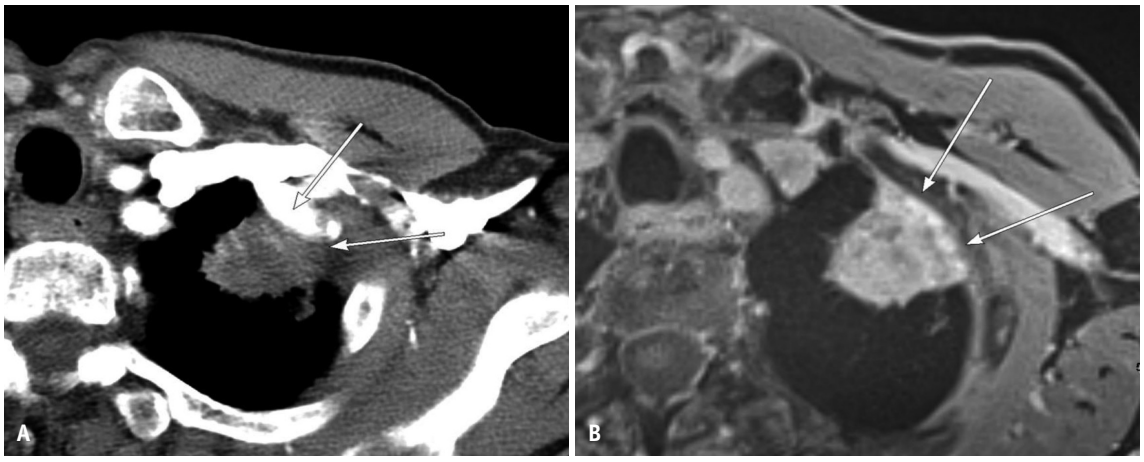

Fig. 6. A 75-year-old male with left upper lobe lung adenocarcinoma and pathologically determined visceral pleural surface invasion (PL2, as determined pathologically).
A. Axial contrast-enhanced CT does not clearly show the interface between tumor and pleura (arrows), highlighting the difficulty in evaluation of pleural invasion by CT. **B.** Post-contrast radial volumetric interpolated breath-hold examination fat-saturated image shows an irregular undulating margin (arrows) of the tumor interface with the pleura, closely abutting the intercostal muscle, and irregular thickening of the enhanced pleura adjacent to the tumor. CT = computed tomography

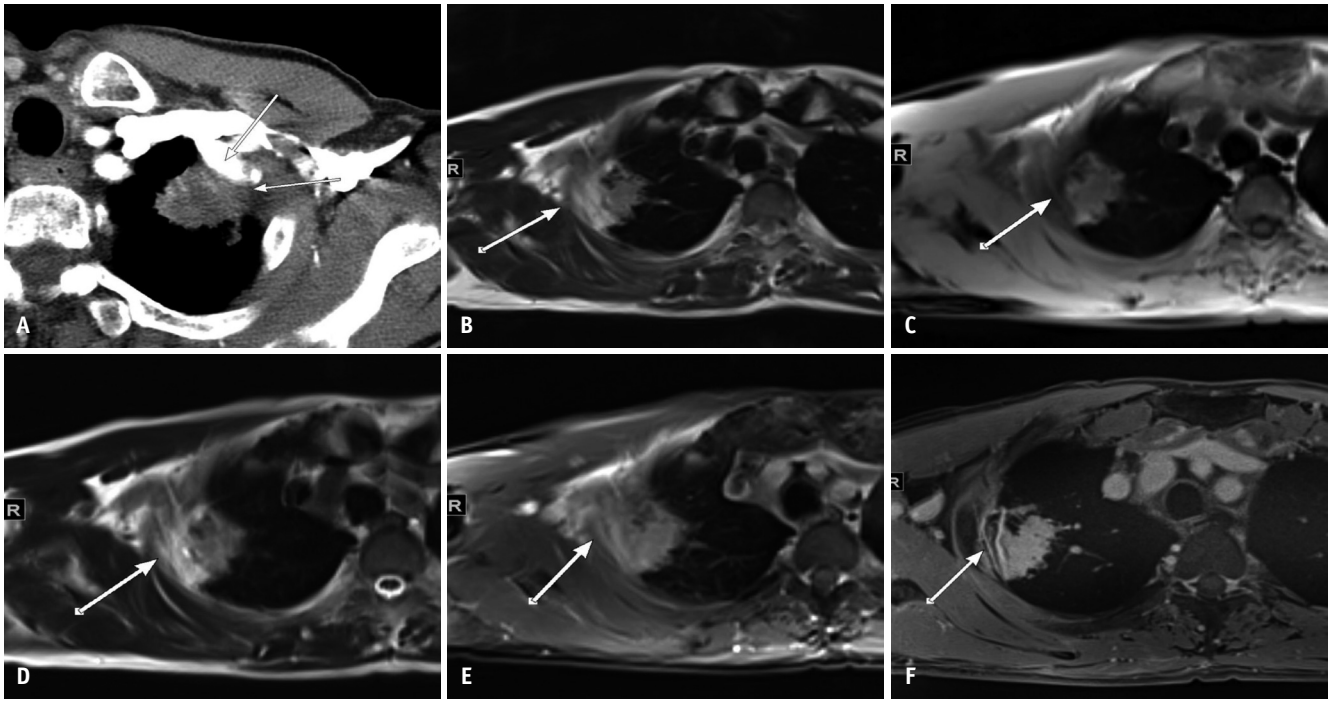

Fig. 7. A 64-year-old male with right upper lobe adenocarcinoma and no visceral pleural surface invasion (PL1, as determined pathologically).
A-C. In the non-contrast breath-hold T1-weighted **(A)**, breath-hold T2-weighted **(B)**, and axial fat-saturated T1-weighted breath-hold **(C)** images, the tumor exhibits a broad interface with the pleura (arrows) but no specific features for pleural invasion. **D, E.** In axial T2-weighted half-Fourier acquisition single-shot turbo spin-echo **(D)** and axial contrast-enhanced T1-weighted fat-suppressed images **(E)**, the interface between the tumor and the pleura is blurred (arrows); however, there is no obvious morphologic sign enabling distinction between visceral pleural surface invasion and the lack thereof. **F.** On contrast-enhanced free-breathing radial volumetric interpolated breath-hold examination imaging, there is a smooth interface of the tumor with the pleura and well-defined, smooth, curvilinear pleural enhancement along the tumor (arrow).

https://doi.org/10.3348/kjr.2020.0955

with no parietal pleural involvement of the tumor [22]. Difficulties in distinguishing tumor invasion from non-malignant, inflammatory adhesions to the pleura and chest wall have been encountered with other diagnostic approaches also, including expiratory dynamic CT [13,23], ultrasound [24], pneumothorax CT [25], and dynamic cine MRI [18,26]. Therefore, this limitation is considered a common problem. This type of inflammatory adhesion was found on pathological examination in the two patients with false-positive MRI findings. MRI with non-contrast T1- and T2-weighted and post-contrast pulse sequences utilized to evaluate these two patients showed an indistinct margin between the tumor and the pleura, leading to the false-positive VPSI classification (Fig. 7).

Several other limitations should be mentioned. First, our study was retrospective in design. The diagnostic performances of other MRI pulse sequences could not be evaluated because only two pulse sequences were commonly shared among all MRI examinations. The assessment of the ability of other MRI pulse sequences to identify VPSI would be of value. Second, despite the enrollment of patients from two medical institutions, the number of patients was small, with three patients having PL2 and nine patients having PL3. This was probably because pathological proof was available only for patients who underwent an operation for a potentially resectable lung cancer. Therefore, patient selection bias was inevitable in this study. Further prospective multi-institutional studies with a larger sample size are required.

In conclusion, the diagnostic performance of contrast-enhanced radial T1-weighted gradient-echo 3T MRI and CT was equal in terms of the contact length, angle of mass margin, and arch distance-to-maximum tumor diameter ratio. The advantage of MRI is that it can clearly show the tumor-pleura interface margin, facilitating VPSI detection. Further studies with larger sample sizes are required to verify the clinical utility of MRI for prognostic use in NSCLC patients.

Conflicts of Interest

The authors have no potential conflicts of interest to disclose.

Author Contributions

Conceptualization: Yu Zhang, Woocheol Kwon. Data curation: Sung Min Ko, Yu Zhang, Woocheol Kwon, Honglei Yang, Junhee Han, Ho Yun Lee, Chun Sung Byun. Formal analysis: JunHyeok Lee, Sung Min Ko. Investigation: Yu Zhang, Woocheol Kwon, Junhee Han, Honglei Yang. Methodology: Woocheol Kwon, Sung Min Ko, Junhee Han, Honglei Yang. Project administration: Sung Min Ko, Woocheol Kwon. Resources: Sung Min Ko, Yu Zhang, Woocheol Kwon, Ho Yun Lee. Supervision: Sung Min Ko, Woocheol Kwon, Sang-Ha Kim, Won-Yeon Lee, Soon-Hee Jung, Chun Sung Byun. Validation: Sung Min Ko, Yu Zhang, Woocheol Kwon, Jeanne B. Ackman. Visualization: Sung Min Ko, Yu Zhang, Woocheol Kwon, Jeanne B. Ackman. Writing—original draft: Yu Zhang, Woocheol Kwon, Sung Min Ko, Honglei Yang. Writing—review & editing: Sung Min Ko, Yu Zhang, Woocheol Kwon, Jeanne B. Ackman, Sang-Ha Kim, Won-Yeon Lee, Suk Joong Yong, Soon-Hee Jung.

ORCID iDs

Yu Zhang
https://orcid.org/0000-0002-5742-0685
Woocheol Kwon
https://orcid.org/0000-0003-0397-4364
Ho Yun Lee
https://orcid.org/0000-0001-9960-5648
Sung Min Ko
https://orcid.org/0000-0002-7420-6269
Sang-Ha Kim
https://orcid.org/0000-0002-1763-5366
Won-Yeon Lee
https://orcid.org/0000-0002-5461-6770
Suk Joong Yong
https://orcid.org/0000-0002-1952-7254
Soon-Hee Jung
https://orcid.org/0000-0003-3565-3426
Chun Sung Byun
https://orcid.org/0000-0001-5409-6798
Jun Hyeok Lee
https://orcid.org/0000-0002-7745-3599
Honglei Yang
https://orcid.org/0000-0002-7240-7235
Junhee Han
https://orcid.org/0000-0001-9859-7690
Jeanne B. Ackman
https://orcid.org/0000-0001-5022-9530

REFERENCES

1. Chang YL, Lin MW, Shih JY, Wu CT, Lee YC. The significance of visceral pleural surface invasion in 321 cases of non-small

https://doi.org/10.3348/kjr.2020.0955

cell lung cancers with pleural retraction. *Ann Surg Oncol* 2012;19:3057-3064
2. Feng SH, Yang ST. The new 8th TNM staging system of lung cancer and its potential imaging interpretation pitfalls and limitations with CT image demonstrations. *Diagn Interv Radiol* 2019;25:270-279
3. Goldstraw P, Chansky K, Crowley J, Rami-Porta R, Asamura H, Eberhardt WE, et al. The IASLC lung cancer staging project: proposals for revision of the TNM stage groupings in the forthcoming (eighth) edition of the TNM classification for lung cancer. *J Thorac Oncol* 2016;11:39-51
4. Sakakura N, Mori S, Okuda K, Fukui T, Hatooka S, Shinoda M, et al. Subcategorization of lung cancer based on tumor size and degree of visceral pleural invasion. *Ann Thorac Surg* 2008;86:1084-1090
5. Glazer HS, Duncan-Meyer J, Aronberg DJ, Moran JF, Levitt RG, Sagel SS. Pleural and chest wall invasion in bronchogenic carcinoma: CT evaluation. *Radiology* 1985;157:191-194
6. Ebara K, Takashima S, Jiang B, Numasaki H, Fujino M, Tomita Y, et al. Pleural invasion by peripheral lung cancer: prediction with three-dimensional CT. *Acad Radiol* 2015;22:310-319
7. Hsu JS, Han IT, Tsai TH, Lin SF, Jaw TS, Liu GC, et al. Pleural tags on CT scans to predict visceral pleural invasion of non–small cell lung cancer that does not abut the pleura. *Radiology* 2016;279:590-596
8. Hsu JS, Jaw TS, Yang CJ, Lin SF, Shih MP, Chou SH, et al. Convex border of peripheral non-small cell lung cancer on CT images as a potential indicator of pleural invasion. *Medicine (Baltimore)* 2017;96:e7323
9. Cho HH, Choi YH, Cheon JE, Lee SM, Kim WS, Kim IO, et al. Free-breathing radial 3D fat-suppressed T1-weighted gradient-echo sequence for contrast-enhanced pediatric spinal imaging: comparison with T1-weighted turbo spin-echo sequence. *AJR Am J Roentgenol* 2016;207:177-182
10. Zhang F, Qu J, Zhang H, Liu H, Qin J, Ding Z, et al. Preoperative T staging of potentially resectable esophageal cancer: a comparison between free-breathing radial VIBE and breath-hold Cartesian VIBE, with Histopathological correlation. *Transl Oncol* 2017;10:324-331
11. Lee H, Choi E, Lee MK, Zhang Y, Kwon W. Morphologic evaluation of primary non-small cell lung cancer by 3 tesla MRI with free-breathing ultrashort echo time and radial T1-weighted gradient echo sequences: a comparison with CT analysis. *J Korean Soc Radiol* 2019;80:466-476
12. Herman SJ, Winton TL, Weisbrod GL, Towers MJ, Mentzer SJ. Mediastinal invasion by bronchogenic carcinoma: CT signs. *Radiology* 1994;190:841-846
13. Glazer HS, Kaiser LR, Anderson DJ, Molina PL, Emami B, Roper CL, et al. Indeterminate mediastinal invasion in bronchogenic carcinoma: CT evaluation. *Radiology* 1989;173:37-42
14. Imai K, Minamiya Y, Ishiyama K, Hashimoto M, Saito H, Motoyama S, et al. Use of CT to evaluate pleural invasion in non-small cell lung cancer: measurement of the ratio of the interface between tumor and neighboring structures to maximum tumor diameter. *Radiology* 2013;267:619-626
15. Travis WD, Brambilla E, Rami-Porta R, Vallières E, Tsuboi M, Rusch V, et al. Visceral pleural invasion: pathologic criteria and use of elastic stains: proposal for the 7th edition of the TNM classification for lung cancer. *J Thorac Oncol* 2008;3:1384-1390
16. Kundel HL, Polansky M. Measurement of observer agreement. *Radiology* 2003;228:303-308
17. Bai JH, Hsieh MS, Liao HC, Lin MW, Chen JS. Prediction of pleural invasion using different imaging tools in non-small cell lung cancer. *Ann Transl Med* 2019;7:33
18. Akata S, Kajiwara N, Park J, Yoshimura M, Kakizaki D, Abe K, et al. Evaluation of chest wall invasion by lung cancer using respiratory dynamic MRI. *J Med Imaging Radiat Oncol* 2008;52:36-39
19. Tsuchiya N, Doai M, Usuda K, Uramoto H, Tonami H. Non-small cell lung cancer: whole-lesion histogram analysis of the apparent diffusion coefficient for assessment of tumor grade, lymphovascular invasion and pleural invasion. *PLoS One* 2017;12:e0172433
20. Warth A, Muley T, Herpel E, Pfannschmidt J, Hoffmann H, Dienemann H, et al. A histochemical approach to the diagnosis of visceral pleural infiltration by non-small cell lung cancer. *Pathol Oncol Res* 2010;16:119-123
21. Gallagher B, Urbanski SJ. The significance of pleural elastica invasion by lung carcinomas. *Hum Pathol* 1990;21:512-517
22. Shiotani S, Sugimura K, Sugihara M, Kawamitsu H, Yamauchi M, Yoshida M, et al. Diagnosis of chest wall invasion by lung cancer: useful criteria for exclusion of the possibility of chest wall invasion with MR imaging. *Radiat Med* 2000;18:283-290
23. Murata K, Takahashi M, Mori M, Shimoyama K, Mishina A, Fujino S, et al. Chest wall and mediastinal invasion by lung cancer: evaluation with multisection expiratory dynamic CT. *Radiology* 1994;191:251-255
24. Suzuki N, Saitoh T, Kitamura S. Tumor invasion of the chest wall in lung cancer: diagnosis with US. *Radiology* 1993;187:39-42
25. Yokoi K, Mori K, Miyazawa N, Saito Y, Okuyama A, Sasagawa M. Tumor invasion of the chest wall and mediastinum in lung cancer: evaluation with pneumothorax CT. *Radiology* 1991;181:147-152
26. Kajiwara N, Akata S, Uchida O, Usuda J, Ohira T, Kawate N, et al. Cine MRI enables better therapeutic planning than CT in cases of possible lung cancer chest wall invasion. *Lung Cancer* 2010;69:203-208

 https://doi.org/10.3348/kjr.2020.0955